



Propagation of Love waves in a functionally graded piezoelectric material (FGPM) layered composite system

Xiaoshan Cao^a, Feng Jin^b, Insu Jeon^{a,*}, Tian Jian Lu^b

^a School of Mechanical Systems Engineering, Chonnam National University, 300 Yongbong-dong, Buk-gu, Gwangju 500-757, Republic of Korea

^b MOE Key Laboratory for Strength and Vibration, School of Aerospace, Xi'an Jiaotong University, Xi'an 710049, People's Republic of China

ARTICLE INFO

Article history:

Received 8 December 2008

Received in revised form 5 August 2009

Available online 11 August 2009

Keywords:

Love waves

Functionally graded piezoelectric material (FGPM)

Layered composite system

Power series technique

Surface acoustic wave (SAW) devices

ABSTRACT

In this theoretical study, we investigate the propagation of Love waves in a layered structure consisting of two different homogenous piezoelectric materials, an upper layer and a substrate. A functionally graded piezoelectric material (FGPM) buffer layer is in between the upper layer and the substrate. We employ the power series technique to solve the governing differential equations with variable coefficients. The influence of the gradient coefficients of FGPM and the layer thicknesses on the dispersion relations, the electro-mechanical coupling factor, and the stress distributions of Love waves in this structure are investigated. We demonstrate that the low gradient coefficient raises the significant variation of the phase velocity within a certain range of ratios of upper layer thickness to equivalent thickness. The electro-mechanical coupling factor can be increased when the equivalent thickness equals one or two wavelengths, and the discontinuity of the interlaminar stress can be eliminated by the FGPM buffer layer. The theoretical results set guidelines not only for the design of high-performance surface acoustic wave (SAW) devices using the FGPM buffer layer, but also for the measurement of material properties in such FGPM layered structures using Love waves.

© 2009 Elsevier Ltd. All rights reserved.

1. Introduction

Since the invention of the interdigital transducer (IDT) for transmitting and receiving surface acoustic wave (SAW) signals (White and Voltmer, 1965), SAW devices (e.g., filters, delay lines, oscillators, and amplifiers) have found a wide range of engineering applications based on the propagation characteristics of surface waves such as Rayleigh waves and Love waves. Love wave sensors are highly sensitive devices owing to the concentration of acoustic energy within a few wavelengths of the surface. To manufacture such a high performance device, layered structures of functional materials have been adopted. However, if all of the materials in the layered structure are homogenous, discontinuity of the interlaminar stress and high local stress fields can arise around the edge of the laminate, due to material mismatch across the interface. To improve the efficiency and durability of SAW devices, the use of functionally graded piezoelectric material (FGPM) has been considered. As a result, the propagation of Love waves in FGPM layered structures has become a research topic with very practical importance.

For surface waves propagating in an inhomogeneous medium for which the material parameters vary continuously, analytical solutions can be obtained only for some special cases, due to the

complexity of the governing equations. Hence, a variety of different numerical methods have been used to study the propagation of waves in functionally graded material (FGM) structures, including FGM structures. By applying the strip element method, Liu et al. (1991) investigated surface waves propagating in a FGM plate. Subsequently, Liu et al. (1999) and Han et al. (2000) addressed stress waves in FGMs with linearly inhomogeneous elements and quadratic layer elements, respectively. Han et al. (2001, 2002) introduced a hybrid numerical method for analyzing the characteristics of waves and transient responses in FGM cylinders. As this method can also be used to solve wave propagation in FGPM structures, Liu et al. (2003) and Han and Liu (2003) later investigated the frequency and group velocity dispersion behaviors and the characteristics of surface waves in FGPM plates and cylinders. Wang and Varadan (2002) studied wave propagation in piezoelectric coupled plates by the reverberation matrix method (RMM). Numerical techniques employed for studying wave propagation in FGPM structures, such as the finite element method (FEM) and reverberation matrix method, typically assume that the FGPM has a multi-layer structure, with each layer taken as homogenous.

The asymptotic analysis of wave propagation in FGPM layered structures has also been reported. Using the Wentzel–Kramers–Brillouin (WKB) method, Li et al. (2004), Liu et al. (2007) and Qian et al. (2007) analyzed the propagation properties of Love waves in different kinds of FGPM layered structures, Jin et al. (2005)

* Corresponding author. Tel.: +82 62 530 1688; fax: +82 62 530 1689.

E-mail address: i_jeon@chonnam.ac.kr (I. Jeon).

investigated Love waves in a piezoelectric layered structure with inhomogeneous initial stresses, whilst Cao et al. (2008a) presented the dispersion relations of Rayleigh waves in a FGPM half-space. In addition to the WKB method, special functions have been used for unique cases. For example, Du et al. (2007) reported an analytical solution for Love waves in an FGPM layer that is bonded to a semi-infinite homogeneous solid wherein all the material properties vary with the same exponential function. Collet et al. (2006) analyzed Bleustein–Gulyaev (B–G) waves in FGPM structures wherein all the material parameters vary proportionally to the same inhomogeneous function. Cao et al. (2008b) studied the propagation behavior of horizontal shear waves in a FGPM plate using Airy equations and Airy functions. However, both the WKB method and the use of special functions have limitations: while the former can be used only at high frequencies, the latter can fit only special cases.

In the present study, the problem of Love wave propagation in a FGPM layered composite system is solved analytically. The composite system consists of two different homogenous piezoelectric materials, separated by a FGPM buffer layer, as shown in Fig. 1. The power series technique, a method with high precision and extensive applicability, is employed to solve the governing equations. The dispersion relations of Love waves are obtained, and the effects of the gradient coefficients of FGPM and the geometrical dimensions of the layers upon the dispersion relations, the electromechanical coupling factor, and the stress distributions of Love waves in this structure are quantified.

2. Statement of the problem and governing equations

We consider the propagation of Love waves in a three-layer FGPM composite structure, as shown in Fig. 1. The top layer and the bottom substrate are made of two different kinds of transversely isotropic piezoelectric materials, designated as materials I and II. The top layer has thickness h_0 , and its upper surface is traction free. For SAW devices, the thickness of the substrate is typi-

cally much greater than those of other layers, and hence it is assumed here that the substrate can be treated as a half-space. The middle layer, which acts as a buffer layer with thickness h , is taken to be a functionally graded material compounded by materials I and II. The coordinate system $o-xyz$ is chosen such that the z -axis is directed along the poling direction perpendicular to the x - y plane; the $x = 0$ plane lies at the boundary between the top layer and the FGPM layer; and the x -axis points down into the substrate (Fig. 1). The mechanical and electrical properties of the functionally graded material vary continuously along the x -axis direction. Without loss of generality, it is further assumed that the Love waves propagate in the positive direction of the y -axis.

The piezoelectric constitutive equations can be expressed as

$$\sigma_{ij} = c_{ijkl}S_{kl} - e_{kij}E_k, \quad (1)$$

$$D_j = e_{jkl}S_{kl} + \epsilon_{jk}E_k, \quad (2)$$

where σ_{ij} and S_{kl} are the stress and strain tensors, D_j and E_k are the electrical displacement and the electrical field intensity and c_{ijkl} , e_{kij} , ϵ_{jk} are the elastic, piezoelectric and dielectric coefficients, respectively. For the FGPM buffer layer, the relevant material properties vary continuously along the thickness direction, i.e., they are functions of the x -axis.

The motion equation and the electrical displacement equilibrium equation are given by

$$\sigma_{ijj} = \rho \ddot{u}_i, \quad (3)$$

$$D_{i,i} = 0, \quad (4)$$

where ρ is the mass density and u_i is the component of mechanical displacement in the i th direction. The comma followed by the subscript i indicates space differentiation with respect to the corresponding coordinate, x_i and the dot “•” represents time differentiation, and the repeated index in the subscript implies summation with respect to that index.

The relation between the mechanical displacement and the strain components is as follows:

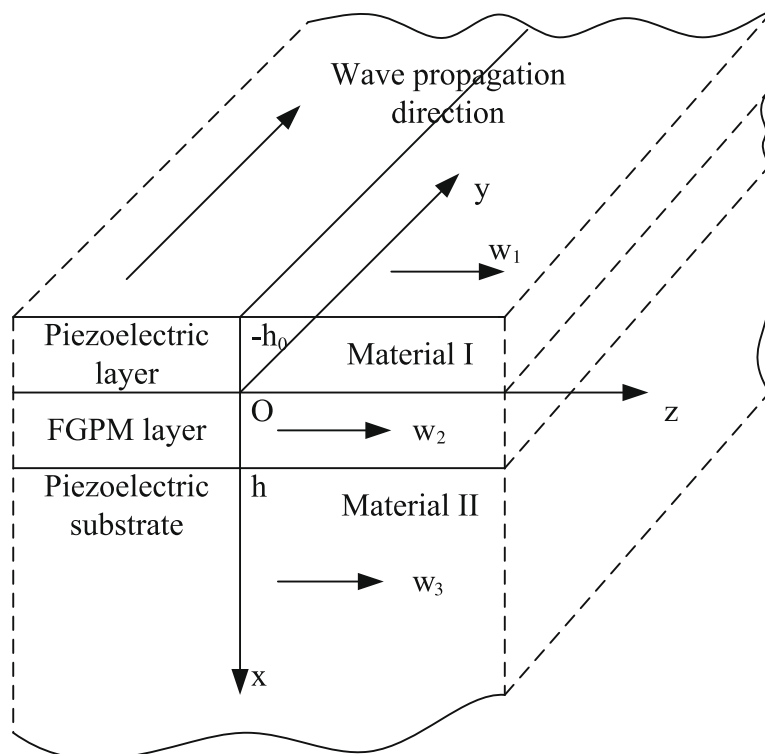


Fig. 1. FGPM layered structure and Cartesian coordinates.

$$S_{ij} = \frac{1}{2}(u_{i,j} + u_{j,i}). \quad (5)$$

According to the quasi-static Maxwell's equation, the relation between the electrical intensity and the electrical potential is

$$E_i = -\frac{\partial \varphi}{\partial x_i}, \quad (6)$$

where φ is the electrical potential function.

Let u , v and w denote the mechanical displacement components. For Love waves propagating in the FGPM layered structure along the y -axis in the positive direction, as shown in Fig. 1, the mechanical displacement components and the electrical potential can be expressed as

$$u = v = 0, \quad w = w(x, y, t), \quad \varphi = \varphi(x, y, t). \quad (7)$$

Typically, for the transversely isotropic piezoelectric layer, Eqs. (1) and (2) can be expressed in the rectangular form as

$$\begin{aligned} \sigma_x &= c_{11}S_x + c_{12}S_y + c_{13}S_z - e_{31}E_z, \\ \sigma_y &= c_{12}S_x + c_{11}S_y + c_{13}S_z - e_{31}E_z, \\ \sigma_z &= c_{13}S_x + c_{13}S_y + c_{33}S_z - e_{31}E_z, \\ \tau_{yz} &= c_{44}S_{yz} - e_{15}E_y, \\ \tau_{xz} &= c_{44}S_{xz} - e_{15}E_x, \\ \tau_{xy} &= (c_{11} - c_{12})S_{xy}/2, \\ D_x &= e_{15}S_{xz} + \varepsilon_{11}E_x, \\ D_y &= e_{15}S_{yz} + \varepsilon_{11}E_y, \\ D_z &= e_{31}S_x + e_{31}S_y + e_{33}S_z + \varepsilon_{33}E_z. \end{aligned} \quad (8)$$

Upon the following sequence of substitutions: (i) Eq. (7) into Eqs. (5) and (6), (ii) the modified equations (5) and (6) into Eq. (8) and (iii) the new equations into Eqs. (3) and (4), the governing equations for the mechanical displacements and the electrical potential can be obtained.

Let w_1 and φ_1 denote the mechanical displacement and the electrical potential in the upper layer, respectively. The governing equations for Love waves propagating in the upper layer ($-h_0 < x < 0$) can be expressed as

$$\bar{c}_{44} \left(\frac{\partial^2 w_1}{\partial x^2} + \frac{\partial^2 w_1}{\partial y^2} \right) + \bar{e}_{15} \left(\frac{\partial^2 \varphi_1}{\partial x^2} + \frac{\partial^2 \varphi_1}{\partial y^2} \right) = \bar{\rho} \frac{\partial^2 w_1}{\partial t^2}, \quad (9)$$

$$\bar{e}_{15} \left(\frac{\partial^2 w_1}{\partial x^2} + \frac{\partial^2 w_1}{\partial y^2} \right) - \bar{\varepsilon}_{11} \left(\frac{\partial^2 \varphi_1}{\partial x^2} + \frac{\partial^2 \varphi_1}{\partial y^2} \right) = 0, \quad (10)$$

where the “ $\bar{\cdot}$ ” symbol is used to denote the parameters associated with the upper layer material.

Similarly, representing the mechanical displacement and the electrical potential in the FGPM buffer layer by w_2 and φ_2 , respectively, we can obtain the governing equations in the FGPM layer ($0 < x < h$):

$$\begin{aligned} c_{44} \left(\frac{\partial^2 w_2}{\partial x^2} + \frac{\partial^2 w_2}{\partial y^2} \right) + e_{15} \left(\frac{\partial^2 \varphi_2}{\partial x^2} + \frac{\partial^2 \varphi_2}{\partial y^2} \right) \\ + c'_{44} \frac{\partial w_2}{\partial x} + e'_{15} \frac{\partial \varphi_2}{\partial x} = \rho \frac{\partial^2 w_2}{\partial t^2}, \end{aligned} \quad (11)$$

$$e_{15} \left(\frac{\partial^2 w_2}{\partial x^2} + \frac{\partial^2 w_2}{\partial y^2} \right) - \varepsilon_{11} \left(\frac{\partial^2 \varphi_2}{\partial x^2} + \frac{\partial^2 \varphi_2}{\partial y^2} \right) + e'_{15} \frac{\partial w_2}{\partial x} - \varepsilon'_{11} \frac{\partial \varphi_2}{\partial x} = 0, \quad (12)$$

where the superscript “ \prime ” indicates space differentiation with respect to the x -coordinate.

Finally, the governing equations in the piezoelectric substrate ($x > h$) are derived as

$$\hat{c}_{44} \left(\frac{\partial^2 w_3}{\partial x^2} + \frac{\partial^2 w_3}{\partial y^2} \right) + \hat{e}_{15} \left(\frac{\partial^2 \varphi_3}{\partial x^2} + \frac{\partial^2 \varphi_3}{\partial y^2} \right) = \hat{\rho} \frac{\partial^2 w_3}{\partial t^2}, \quad (13)$$

$$\hat{e}_{15} \left(\frac{\partial^2 w_3}{\partial x^2} + \frac{\partial^2 w_3}{\partial y^2} \right) - \hat{\varepsilon}_{11} \left(\frac{\partial^2 \varphi_3}{\partial x^2} + \frac{\partial^2 \varphi_3}{\partial y^2} \right) = 0, \quad (14)$$

where w_3 and φ_3 are the mechanical displacement and the electrical potential in the substrate, and the symbol “ $\hat{\cdot}$ ” is used to denote the parameters associated with the substrate material.

The electrical potential φ_0 in the air above the upper layer should satisfy the Laplace equation, i.e., for $x < -h_0$:

$$\frac{\partial^2 \varphi_0}{\partial x^2} + \frac{\partial^2 \varphi_0}{\partial y^2} = 0. \quad (15)$$

For Love waves propagating in the FGPM layered structure considered here, the following boundary conditions and interface continuity conditions should be satisfied:

(a) Traction free boundary condition:

$$\tau_{xz}(-h_0, y) = 0 \quad \text{at } x = -h_0.$$

(b) Electrical boundary conditions:

$$D_{x1}(-h_0, y) = D_{x0}(-h_0, y),$$

$$\varphi_1(-h_0, y) = 0 \quad \text{for the electrically shorted case,}$$

$$\varphi_1(-h_0, y) = \varphi_0(-h_0, y) \quad \text{for the electrically open case.}$$

(c) Along the interfaces between the upper layer and the FGPM layer, and between the FGPM layer and the substrate, the stress, mechanical displacement, electrical potential and electrical displacement are all continuous:

$$w_1(0, y) = w_2(0, y), \quad \tau_{xz1}(0, y) = \tau_{xz2}(0, y),$$

$$\varphi_1(0, y) = \varphi_2(0, y), \quad D_{x1}(0, y) = D_{x2}(0, y),$$

$$w_2(h, y) = w_3(h, y), \quad \tau_{xz2}(h, y) = \tau_{xz3}(h, y),$$

$$\varphi_2(h, y) = \varphi_3(h, y), \quad D_{x2}(h, y) = D_{x3}(h, y).$$

(d) The attenuation conditions for Love waves at $x \rightarrow \pm\infty$ are

$$\varphi_3 \rightarrow 0, \quad w_3 \rightarrow 0 \quad \text{as } x \rightarrow +\infty,$$

$$\varphi_0 \rightarrow 0 \quad \text{as } x \rightarrow -\infty.$$

In the above equations, the subscripts 0, 1, 2 and 3 are used to denote the mechanical and electrical quantities in the air, the upper layer, the FGPM layer and the substrate, respectively.

3. Solution of the problem

For Love waves propagating in the FGPM layered structure described above, the solutions of the governing equations can be expressed as

$$w_j(x, y, t) = W_j(x) \exp[ik(y - ct)], \quad (16)$$

$$\varphi_j(x, y, t) = \Phi_j(x) \exp[ik(y - ct)], \quad (17)$$

where $i = \sqrt{-1}$, j ($= 1, 2, 3$) represents the j th layer, $k = 2\pi/\lambda$ is the wave number (λ being the wavelength), c is the phase velocity and

$W_j(x)$ and $\Phi_j(x)$ are the amplitudes of the mechanical displacement and the electrical potential that are to be solved, respectively.

First, the governing equations in the FGPM buffer layer can be solved by substituting Eqs. (16) and (17) into Eqs. (11) and (12), respectively, yielding the following:

$$c_{44}(W_2'' - k^2 W_2) + e_{15}(\Phi_2'' - k^2 \Phi_2) + c'_{44}W_2' + e'_{15}\Phi_2' + \rho c^2 k^2 W_2 = 0, \tag{18}$$

$$e_{15}(W_2'' - k^2 W_2) - \varepsilon_{11}(\Phi_2'' - k^2 \Phi_2) + e'_{15}W_2' - \varepsilon'_{11}\Phi_2' = 0. \tag{19}$$

It is assumed that the material parameters of the FGPM layer are of the following functional form:

$$c_{44} = \sum_{n=0}^{\infty} a_n^1 \left(\frac{x}{h}\right)^n, \quad \rho = \sum_{n=0}^{\infty} a_n^2 \left(\frac{x}{h}\right)^n, \quad e_{15} = \sum_{n=0}^{\infty} a_n^3 \left(\frac{x}{h}\right)^n, \tag{20}$$

$$\varepsilon_{11} = \sum_{n=0}^{\infty} a_n^4 \left(\frac{x}{h}\right)^n,$$

where the coefficients a_n^i can be determined by the relations between the functions and their Taylor expansions. In view of the material grading relations given in Eq. (20), the solutions of Eqs. (18) and (19) can be assumed to take similar forms:

$$W_2 = \sum_{n=0}^{\infty} s_n \left(\frac{x}{h}\right)^n, \quad \Phi_2 = \sum_{n=0}^{\infty} t_n \left(\frac{x}{h}\right)^n. \tag{21}$$

Substitution of (20) and (21) into (18) and (19), respectively, leads to

$$\left(\sum_{n=0}^{\infty} (n+2)(n+1)s_{n+2} \left(\frac{x}{h}\right)^n - (kh)^2 \sum_{n=0}^{\infty} s_n \left(\frac{x}{h}\right)^n \right) \sum_{n=0}^{\infty} a_n^1 \left(\frac{x}{h}\right)^n + \sum_{n=0}^{\infty} (n+1)a_{n+1}^1 \left(\frac{x}{h}\right)^n \sum_{n=0}^{\infty} (n+1)s_{n+1} \left(\frac{x}{h}\right)^n + c^2(kh)^2 \times \sum_{n=0}^{\infty} a_n^2 \left(\frac{x}{h}\right)^n \sum_{n=0}^{\infty} s_n \left(\frac{x}{h}\right)^n + \sum_{n=0}^{\infty} (n+1)a_{n+1}^2 \left(\frac{x}{h}\right)^n \sum_{n=0}^{\infty} (n+1)t_{n+1} \left(\frac{x}{h}\right)^n + \left(\sum_{n=0}^{\infty} (n+2)(n+1)t_{n+2} \left(\frac{x}{h}\right)^n - (kh)^2 \sum_{n=0}^{\infty} t_n \left(\frac{x}{h}\right)^n \right) \sum_{n=0}^{\infty} a_n^3 \left(\frac{x}{h}\right)^n = 0, \tag{22}$$

$$\left(\sum_{n=0}^{\infty} (n+2)(n+1)s_{n+2} \left(\frac{x}{h}\right)^n - (kh)^2 \sum_{n=0}^{\infty} s_n \left(\frac{x}{h}\right)^n \right) \sum_{n=0}^{\infty} a_n^3 \left(\frac{x}{h}\right)^n + \sum_{n=0}^{\infty} (n+1)a_{n+1}^3 \left(\frac{x}{h}\right)^n \sum_{n=0}^{\infty} (n+1)s_{n+1} \left(\frac{x}{h}\right)^n - \sum_{n=0}^{\infty} (n+1)a_{n+1}^4 \left(\frac{x}{h}\right)^n \sum_{n=0}^{\infty} (n+1)t_{n+1} \left(\frac{x}{h}\right)^n - \left(\sum_{n=0}^{\infty} (n+2)(n+1)t_{n+2} \left(\frac{x}{h}\right)^n - (kh)^2 \sum_{n=0}^{\infty} t_n \left(\frac{x}{h}\right)^n \right) \sum_{n=0}^{\infty} a_n^4 \left(\frac{x}{h}\right)^n = 0. \tag{23}$$

By equating the coefficients of $(x/h)^n$ in Eqs. (22) and (23) to zero, we obtain two recursive equations for s_n and t_n , as shown below:

$$\sum_{i=0}^n a_{n-i}^1 [(i+2)(i+1)s_{i+2} - (kh)^2 s_i] + \sum_{i=0}^n (n-i+1)(i+1)a_{n-i+1}^1 s_{i+1} + c^2(kh)^2 \sum_{i=0}^n a_{n-i}^2 s_i + \sum_{i=0}^n (n-i+1)(i+1)a_{n-i+1}^3 t_{i+1} + \sum_{i=0}^n a_{n-i}^3 [(i+2)(i+1)t_{i+2} - (kh)^2 t_i] = 0, \tag{24}$$

$$\sum_{i=0}^n a_{n-i}^3 [(i+2)(i+1)s_{i+2} - (kh)^2 s_i] + \sum_{i=0}^n (n-i+1)(i+1)a_{n-i+1}^3 s_{i+1} - \sum_{i=0}^n (n-i+1)(i+1)a_{n-i+1}^4 t_{i+1} - \sum_{i=0}^n a_{n-i}^4 [(i+2)(i+1)t_{i+2} - (kh)^2 t_i] = 0. \tag{25}$$

Eqs. (24) and (25) describe a series of the linear recursive relations of s_n and t_n with n from zero to infinite. Here, s_0, s_1, t_0 and t_1 are the coefficients to be determined and, for $i \geq 2, s_i$ and t_i are all linear functions of s_0, s_1, t_0 and t_1 . For example, by equating the coefficients of $(x/h)^0$ in Eqs. (22) and (23) to zero, we obtain the first recursive equations of Eqs. (24) and (25) (with corresponding to the case of $n = 0$), which describe the linear relation of s_0, s_1, t_0, t_1, s_2 and t_2 . Therefore, s_2 and t_2 can be solved as the linear function of these unknown coefficients.

To decouple the unknown coefficients, the following matrix is introduced:

$$(s_{0j}, s_{1j}, t_{0j}, t_{1j}) = I, \tag{26}$$

where $j = 1-4$ and I is a 4×4 unit matrix. Accordingly, Eq. (21) can be rewritten as

$$W_2 = \sum_{j=1}^4 C_j \sum_{n=0}^{\infty} s_{nj} \left(\frac{x}{h}\right)^n, \quad \Phi_2 = \sum_{j=1}^4 C_j \sum_{n=0}^{\infty} t_{nj} \left(\frac{x}{h}\right)^n, \tag{27}$$

where the constants C_j ($j = 1-4$) are to be determined. For $n = 0$ and 1, both s_{nj} and t_{nj} are determined by (26). For other values of n, s_{nj} and t_{nj} can be determined by solving Eqs. (24) and (25), while in these recursive equations, s_{nj} and t_{nj} are replaced by s_n and t_n .

By substituting Eqs. (16) and (17) into Eqs. (9) and (10), the mechanical displacements and the electrical potential functions in the upper layer and the substrate can be solved. Let the bulk shear wave velocity \bar{c}_{sh} in the piezoelectric upper layer be defined as

$$\bar{c}_{sh} = \sqrt{(\bar{c}_{44} + \bar{e}_{15}^2/\bar{\varepsilon}_{11})/\bar{\rho}}.$$

When $c > \bar{c}_{sh}$, the solutions of (9) and (10) are

$$w_1(x, y, t) = [C_5 \cos(k\bar{q}_1 x) + C_6 \sin(k\bar{q}_1 x)] \exp[ik(y - ct)], \tag{28}$$

$$\varphi_1(x, y, t) = \left\{ \frac{\bar{e}_{15}}{\bar{\varepsilon}_{11}} [C_5 \cos(k\bar{q}_1 x) + C_6 \sin(k\bar{q}_1 x)] + C_7 e^{-kx} + C_8 e^{kx} \right\} \times \exp[ik(y - ct)], \tag{29}$$

where $\bar{q}_1 = \sqrt{c^2/\bar{c}_{sh}^2 - 1}$ and C_j ($j = 5-8$) are undetermined constants. For $c < \bar{c}_{sh}$, the solutions of (9) and (10) become

$$w_1(x, y, t) = [C_5 e^{-k\bar{q}_2 x} + C_6 e^{k\bar{q}_2 x}] \exp[ik(y - ct)], \tag{30}$$

$$\varphi_1(x, y, t) = \left[\frac{\bar{e}_{15}}{\bar{\varepsilon}_{11}} (C_5 e^{-k\bar{q}_2 x} + C_6 e^{k\bar{q}_2 x}) + C_7 e^{-kx} + C_8 e^{kx} \right] \exp[ik(y - ct)], \tag{31}$$

where $\bar{q}_2 = \sqrt{1 - c^2/\bar{c}_{sh}^2}$ and C_j ($j = 5-8$) are undetermined constants.

For the substrate medium, $\varphi_3 \rightarrow 0$ and $w_3 \rightarrow 0$ as $x \rightarrow \infty$, and hence the solutions of (13) and (14) are given by

$$w_3(x, y, t) = C_9 e^{-k\bar{q}x} \exp[ik(y - ct)], \tag{32}$$

$$\varphi_3(x, y, t) = \left(\frac{\hat{e}_{15}}{\hat{\varepsilon}_{11}} C_9 e^{-k\hat{q}x} + C_{10} e^{-kx} \right) \exp[ik(y - ct)], \quad (33)$$

where $\hat{q} = \sqrt{1 - c^2/\hat{c}_{sh}^2}$ and C_j ($j = 9-10$) are undetermined constants. Here, $\hat{c}_{sh} = \sqrt{(\hat{c}_{44} + \hat{e}_{15}^2/\hat{\varepsilon}_{11})/\hat{\rho}}$ is the bulk shear wave velocity in the substrate.

For the air above the top layer, $\varphi_0 \rightarrow 0$ as $x \rightarrow -\infty$, and hence the solution of (15) is

$$\varphi_0(x, y, t) = C_{11} e^{kx} \exp[ik(y - ct)], \quad (34)$$

where the constant C_{11} is yet to be determined.

By substituting Eq. (27)–(34) into the boundary conditions and continuity conditions for the electrically open case, we obtain a set of homogeneous linear algebraic equations to determine C_i ($i = 1-11$). The sufficient and necessary condition for the existence of a non-trivial solution is that the determinant of the coefficient matrix has to vanish. For the electrically open case:

$$|Q_{ij}^o| = 0, \quad i, j = 1-11, \quad (35)$$

which leads to the dispersion relation for the Love wave. For $c > \hat{c}_{sh}$, we have

$$Q_{15}^o = k\bar{q}_1 (\bar{c}_{44} + \bar{e}_{15}^2/\bar{\varepsilon}_{11}) \sin(k\bar{q}_1 h_0),$$

$$Q_{16}^o = k\bar{q}_1 (\bar{c}_{44} + \bar{e}_{15}^2/\bar{\varepsilon}_{11}) \cos(k\bar{q}_1 h_0),$$

$$Q_{17}^o = -k\bar{e}_{15} e^{k h_0}, \quad Q_{18}^o = k\bar{e}_{15} e^{-k h_0},$$

$$Q_{22}^o = \frac{c_{44}^o}{h}, \quad Q_{24}^o = \frac{e_{15}^o}{h}, \quad Q_{26}^o = -k\bar{q}_1 (\bar{c}_{44} + \bar{e}_{15}^2/\bar{\varepsilon}_{11}),$$

$$Q_{27}^o = k\bar{e}_{15}, \quad Q_{28}^o = -k\bar{e}_{15},$$

$$Q_{31}^o = 1, \quad Q_{35}^o = -1,$$

$$Q_{43}^o = 1, \quad Q_{45}^o = -\frac{\bar{e}_{15}}{\bar{\varepsilon}_{11}}, \quad Q_{47}^o = -1, \quad Q_{48}^o = -1,$$

$$Q_{52}^o = \frac{e_{15}^o}{h}, \quad Q_{54}^o = -\frac{e_{11}^o}{h}, \quad Q_{57}^o = -k\bar{e}_{11}, \quad Q_{58}^o = k\bar{e}_{11},$$

$$Q_{6j}^o = c_{44}^h \sum_{n=0}^{\infty} \frac{(n+1)}{h} s_{nj} + e_{15}^h \sum_{n=0}^{\infty} \frac{(n+1)}{h} t_{nj}, \quad j = 1-4,$$

$$Q_{69}^o = \left(\hat{c}_{44} + \frac{\hat{e}_{15}^2}{\hat{\varepsilon}_{11}} \right) k\hat{q} e^{-k\hat{q}h}, \quad Q_{6-10}^o = \hat{e}_{15} k e^{-kh},$$

$$Q_{7j}^o = \sum_{n=0}^{\infty} s_{nj}, \quad j = 1-4, \quad Q_{79}^o = -e^{-k\hat{q}h},$$

$$Q_{8j}^o = \sum_{n=0}^{\infty} t_{nj}, \quad j = 1-4, \quad Q_{89}^o = -\frac{\hat{e}_{15}}{\hat{\varepsilon}_{11}} e^{-k\hat{q}h}, \quad Q_{8-10}^o = -e^{-kh},$$

$$Q_{9j}^o = e_{15}^h \sum_{n=0}^{\infty} \frac{(n+1)}{h} s_{nj} - \varepsilon_{11}^h \sum_{n=0}^{\infty} \frac{(n+1)}{h} t_{nj}, \quad j = 1-4,$$

$$Q_{9-10}^o = -\hat{e}_{11} k e^{-kh},$$

$$Q_{10-5}^o = \frac{\bar{e}_{15}}{\bar{\varepsilon}_{11}} \cos(k\bar{q}_1 h_0), \quad Q_{10-6}^o = -\frac{\bar{e}_{15}}{\bar{\varepsilon}_{11}} \sin(k\bar{q}_1 h_0),$$

$$Q_{10-7}^o = e^{k h_0}, \quad Q_{10-8}^o = e^{-k h_0}, \quad Q_{10-11}^o = -e^{-k h_0},$$

$$Q_{11-7}^o = k\bar{e}_{11} e^{k h_0}, \quad Q_{11-8}^o = -k\bar{e}_{11} e^{-k h_0}, \quad Q_{11-11}^o = \varepsilon_0 k e^{-k h_0}$$

All the other terms in (35) are equal to zero. The superscript 0 and h denote the material parameters of the top and bottom surfaces of the FGPM layer, respectively.

Again, with Eq. (35), for $c < \bar{c}_{sh}$ we have

$$Q_{15}^o = -k\bar{q}_2 (\bar{c}_{44} + \bar{e}_{15}^2/\bar{\varepsilon}_{11}) e^{k\bar{q}_2 h_0}, \quad Q_{16}^o = k\bar{q}_2 (\bar{c}_{44} + \bar{e}_{15}^2/\bar{\varepsilon}_{11}) e^{-k\bar{q}_2 h_0},$$

$$Q_{25}^o = k\bar{q}_2 (\bar{c}_{44} + \bar{e}_{15}^2/\bar{\varepsilon}_{11}), \quad Q_{26}^o = -k\bar{q}_2 (\bar{c}_{44} + \bar{e}_{15}^2/\bar{\varepsilon}_{11}),$$

$$Q_{35}^o = -1, \quad Q_{36}^o = -1, \quad Q_{45}^o = -\frac{\bar{e}_{15}}{\bar{\varepsilon}_{11}}, \quad Q_{46}^o = -\frac{\bar{e}_{15}}{\bar{\varepsilon}_{11}},$$

$$Q_{10-5}^o = \frac{\bar{e}_{15}}{\bar{\varepsilon}_{11}} e^{k\bar{q}h_0}, \quad Q_{10-6}^o = \frac{\bar{e}_{15}}{\bar{\varepsilon}_{11}} e^{-k\bar{q}h_0},$$

and the other terms are identical to those in the case of $c > \bar{c}_{sh}$.

For the electrically shorted case, Eq. (34) and C_{11} are superfluous. As indicated in condition (b), the number of the boundary conditions for the electrically shorted case is one less than that for the electrically open case. Hence, there exists only 10 undetermined coefficients and the Love wave dispersion relation for the electrically shorted case is determined:

$$|Q_{ij}^{sh}| = 0, \quad (36)$$

where the coefficient matrix $[Q_{ij}^{sh}]$ is 10×10 , with $Q_{ij}^{sh} = Q_{ij}^o$, $i, j = 1-10$. Namely, we can obtain the coefficient matrix $[Q_{ij}^{sh}]$ by eliminating the 11th row and column of the coefficient matrix $[Q_{ij}^o]$.

The relations between the phase velocity and wave number for the electrically open and shorted cases can be obtained from Eqs. (35) and (36). Furthermore, the relations between the unknown constants can be obtained from

$$Q_{ij}^o C_j = 0 \quad \text{or} \quad Q_{ij}^{sh} C_j = 0.$$

The distribution of the stresses can be obtained from Eq. (8).

4. Numerical results and discussion

For numerical analysis with the theoretical model developed above, the FGPM middle layer is taken as a functionally graded composite compounded by materials I and II, with their volume fractions varying along the thickness direction and the top and bottom surfaces of the FGPM layer identical to those of material I and material II, respectively. It is assumed that the volume fractions of materials I and II in the FGPM layer can be described as

$$f_1 = 1 - \frac{1 - \exp(px/h)}{1 - \exp(p)}, \quad f_2 = \frac{1 - \exp(px/h)}{1 - \exp(p)}, \quad (37)$$

where p is the gradient coefficient. The variations of f_1 and f_2 with depth x/h are plotted for values of p from -1 to 10 in Fig. 2. It can be seen that the volume fraction of material I (f_1) increases and that of material II (f_2) decreases when the gradient coefficient p is increased, and f_1 and f_2 are linear functions of x/h , when $p = 0$. The parameters associated with the FGPM composite are described as

$$g(x) = g^{(1)} f_1(x) + g^{(2)} f_2(x), \quad (38)$$

where g represents the elastic, piezoelectric, dielectric and other coefficients of the FGPM composite, and $g^{(1)}$ and $g^{(2)}$ represent the corresponding parameters of materials I and II, respectively.

In order to express the wave propagation properties in the same average thickness of the top layer (material I), we define the equivalent thickness of the material I, H , as

$$H = h_0 + \int_0^h f_1(x) dx. \quad (39)$$

The influence of the gradient coefficient, p , and the thickness of the upper layer h_0 , on the propagation properties of Love waves in a structure having the same equivalent thickness, i.e., $H = 0.0005$ m, is discussed below. With the value of H fixed, the thinner the upper layer (h_0), the thicker the FGPM layer (h) becomes.

PZT-2 and ZnO are chosen as materials I and II, respectively, with

$$\bar{c}_{44} = 22.2 \text{ GPa}, \quad \bar{\rho} = 7.600 \times 10^3 \text{ kg/m}^3, \quad \bar{\epsilon}_{15} = 9.80 \text{ C/m}^2, \\ \hat{\epsilon}_{11} = 44.6 \times 10^{-10} \text{ F/m},$$

$$\hat{c}_{44} = 42.3 \text{ GPa}, \quad \hat{\rho} = 5.665 \times 10^3 \text{ kg/m}^3, \quad \hat{\epsilon}_{15} = 0.48 \text{ C/m}^2, \\ \hat{\epsilon}_{11} = 6.70 \times 10^{-11} \text{ F/m}$$

For both materials, the dielectric constant is $\epsilon_0 = 8.854 \times 10^{-12}$ F/m.

It has been established that if the material parameters of the FGPM layer vary slowly, i.e., if $|\frac{g^{(2)} - g^{(1)}}{g^{(1)}}| < 1$, then all the numerical results satisfy the convergence criterion given below:

$$\frac{|c_{|n=N} - c_{|n>N}|}{c_{|n=N}} < \epsilon, \quad (40)$$

where c_n is the solution of the phase velocity that is yielded by the first n terms of the power series. For $\epsilon = 0.001\%$, the convergence criterion (40) can be satisfied with $N = 500$ in all the numerical examples presented in this paper.

4.1. Influence of gradient coefficient and top layer thickness on dispersive curves

To investigate the influence of the inhomogeneous characteristics of FGPM on the propagation properties of Love waves, the relation between phase velocity, c , and wave number, k , is obtained with Eqs. (35) and (36). When $p = 0$, i.e., when all the FGPM parameters vary linearly, the dispersive curves for the electrically open and shorted cases are plotted in Figs. 3 and 4, with

$h_0/H = 0.6$ and $h_0/H = 0.2$, respectively, and kH as the dimensionless wave number. The first and second modes for each case, M1 and M2, correspond to the two smallest roots of the pertinent dispersion relation. For comparison, results for a bilayer structure consisting of material I as the top layer (thickness h_0) and material II as the substrate (half-space) are also included in Figs. 3 and 4.

The results shown in Figs. 3 and 4 demonstrate that the phase velocity of Love waves changes noticeably if there is a FGPM middle layer. For the first mode, in the electrically open case, the rate of change of the phase velocity is significant, as the value of kH increases from 1 to 4, but remains fairly constant when $kH > 4$. Also for the first mode of the electrically shorted case, the phase velocity drops sharply as kH is increased to a value of approximately 1.8. After reaching this value, the rate with which phase velocity drops begins to asymptotically approach zero as kH is further increased. For the second mode, the variation of the phase velocity is similar for both the electrically open and shorted cases. At the beginning, the velocity of the FGPM composite structure is less than that of the bilayer structure until a critical value of kH , at which point the two types of curves cross each other (Figs. 3 and 4). As the value of kH is further increased, the phase velocity of the former exceeds that of the latter.

The results in Figs. 3 and 4 also suggest that the thickness of the FGPM layer significantly affects the dispersion relations. To explore this further, the variation of the phase velocity of the first mode, Δc , is plotted as a function of h_0/H in Fig. 5 for selected values of kH . For $kH = \pi/2$, i.e., when the equivalent thickness H equals one quarter of the wavelength, the change of phase velocity in the electrically shorted case is more obvious than that in the electrically open case. However, the reverse holds when kH equals 2π or 3π , i.e., when the equivalent thickness, H , equals 1 or 1.5 wavelengths.

To highlight the influence of the gradient coefficient on phase velocity, the variation of the phase velocity of the first mode, Δc , is plotted in Fig. 6 as a function of kH for selected values of gradient coefficient p , while Δc is the difference between the value of the phase velocity of Love waves in the FGPM layered structure and in the bilayer structure. It is seen that Δc initially decreases as the value of p is increased from -1 to 1 , then increases sharply with further increase of p , and reaches a maximum when the equivalent thickness H equals 0.2–0.4 wavelengths for the electrically shorted case and 0.5–1 wavelengths for the electrically open case. When

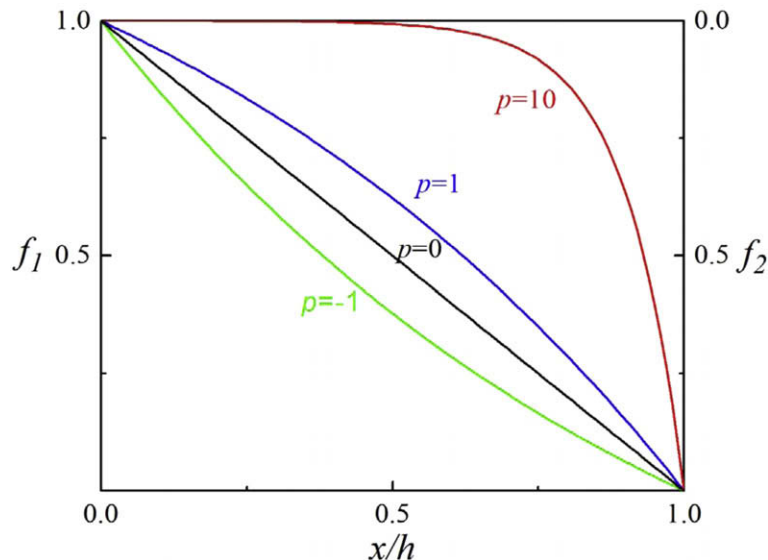


Fig. 2. The profile of volume fraction of material I along the depth.

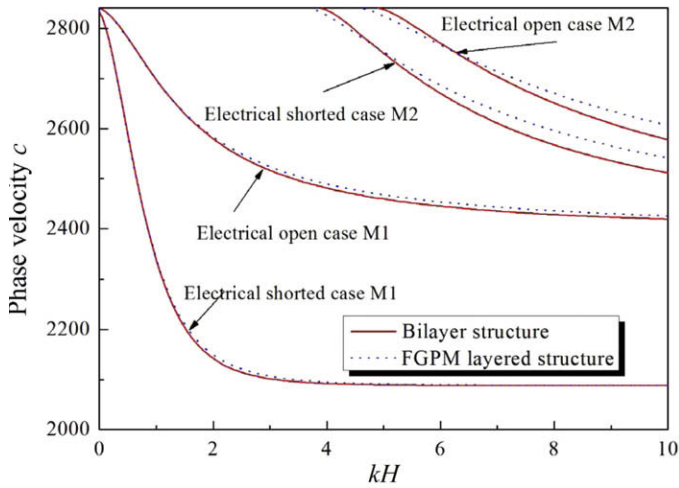


Fig. 3. Comparison of the dispersive relations of Love waves between the FGPM layered structure ($p = 0$, $h_0/H = 0.6$) and the bilayer structure.

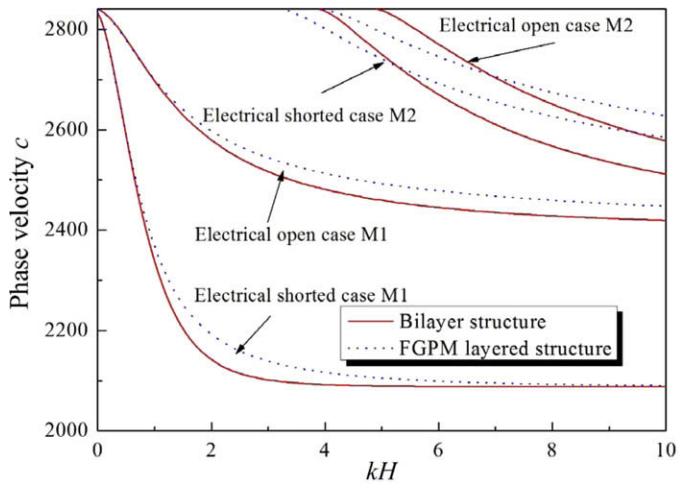


Fig. 4. Comparison of the dispersive relations of Love waves between the FGPM layered structure ($p = 0$, $h_0/H = 0.2$) and the bilayer structure.

the value of p equals -1 , the change in the phase velocity is the most significant (see Fig. 6), which is expected because the distribution of material in the FGPM three-layer structure is distinguishably different from that in the bilayer structure. For large values of the gradient coefficient (e.g., $p = 10$ when the distribution of material in the FGPM three-layer structure is similar to that in the ungraded bilayer structure), the dispersive relations of the two different structures can still be distinguished (especially for small values of kH), due to differences in the continuity of relevant material parameters.

Fig. 7 shows the variation of phase velocity as a function of gradient coefficient, with the value of kH fixed at 2π . It is interesting to see that the relation between Δc and p is approximately linear.

To further investigate the influence of material gradient on dispersion properties, the group velocity of wave propagation is introduced, which is defined as $c_g = c + kdc/dk$ and expresses the rate at which energy is transported. Normally, the dispersion property is determined by the relation between the phase velocity and the group velocity. If the group velocity is actually greater than the phase velocity, the dispersion is termed “anomalous”, and if the converse holds the dispersion is “normal”. By examining the Love wave dispersive curves in Figs. 3 and 4, it is seen that the waves ex-

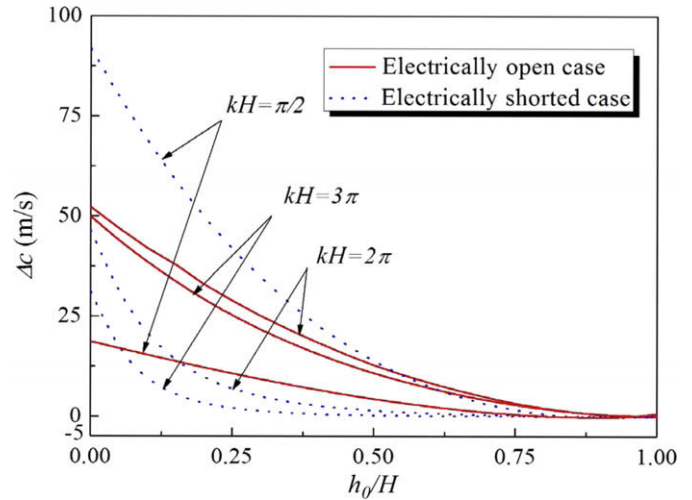


Fig. 5. Relations between the variation of the phase velocity and h_0/H .

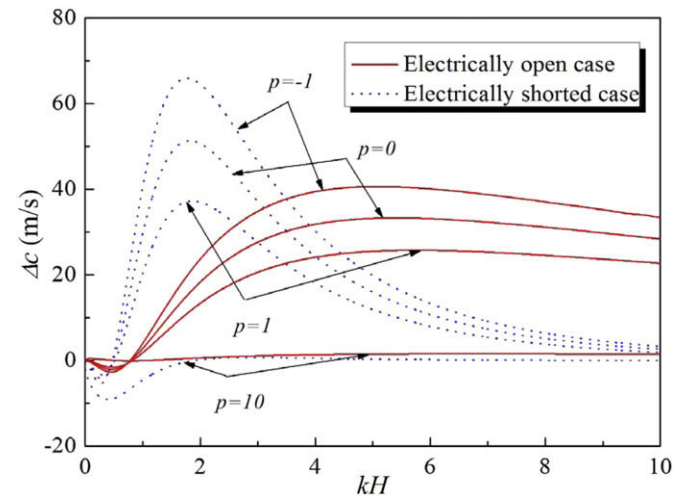


Fig. 6. Comparison of Δc with different p , $h_0/H = 0.2$.

hibit normal dispersion because $dc/dk < 0$. Fig. 8 plots both the phase velocity and the group velocity as functions of kH for the three-layer FGPM structure and the bilayer structure. It is seen that for the electrically open case, the velocity of energy propagation in the FGPM structure is always larger than that in the bilayer structure. For the electrically shorted case, the velocity of energy propagation in the FGPM structure is more than that in the bilayer structure only when $kH > 2.65$.

4.2. Influence of gradient coefficient and top layer thickness on coupled electromechanical factors

For typical engineering applications, both a greater electromechanical coupling factor and a lower penetration depth of the waves are expected in SAW devices. The electromechanical coupling factor for surface waves can be defined as

$$\kappa^2 = 2 \frac{c_o - c_s}{c_o}$$

where c_o and c_s are the phase velocity for the electrically open and electrically shorted cases, respectively. Fig. 9 plots the electromechanical coupling factor as a function of kH for the first two

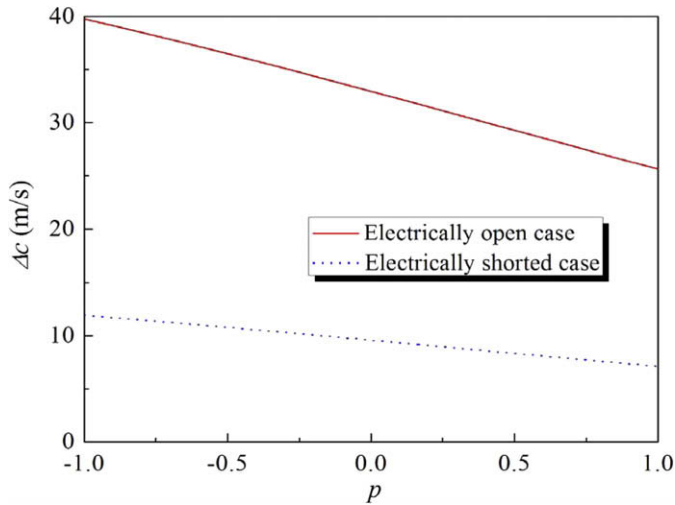


Fig. 7. Relation between Δc and p at $h_0/H = 0.2$ and $kH = 2\pi$.

modes. In comparison, for mode 1, although the presence of a FGPM buffer layer leads to decreased peak values of the factor, it can also increase the factor when kH is larger than approximately 3.8. For mode 2, the presence of a FGPM layer causes the factor to decrease over the range of kH considered here.

It is of particular interest to examine the propagation properties when the non-dimensional thickness of the FGPM layer, h_0/H , is a multiple of the wavelength. The electro-mechanical coupling factor is plotted as a function of h_0/H in Fig. 10 for $p = 0$ and two different values of kH (2π and 3π). The two thin lines in Fig. 10 (i.e., $\kappa^2 = 28.98\%$ and 27.56%) represent the electro-mechanical coupling factor of the bilayer structure for $kH = 2\pi$ and $kH = 3\pi$, respectively. It is seen from Fig. 10 that the electro-mechanical coupling factor of the FGPM composite structure is maximized when h_0/H equals 0.1–0.2. These results should be useful for the practical design of Love wave SAW devices that adopt a FGPM buffer layer.

The influence of the gradient coefficient on the electro-mechanical coupling factor has also been studied, and the results are shown in Fig. 11. From this figure, it can be concluded that the addition of a FGPM layer to a bilayer structure leads to enhanced electro-mechanical coupling factors, but this enhancement effect weakens as the gradient coefficient is increased in magnitude.

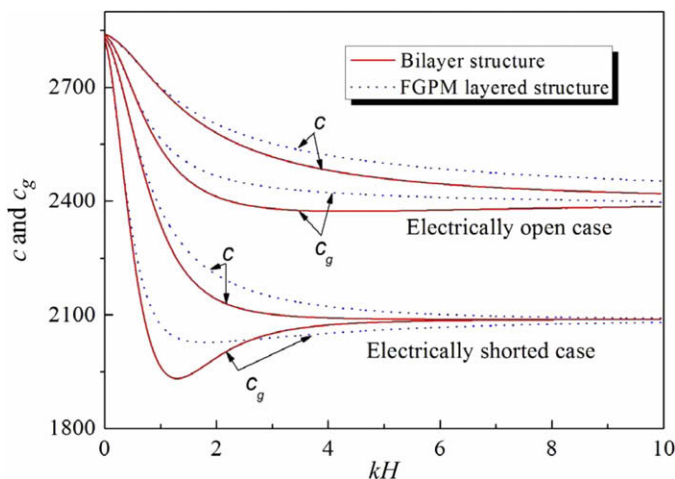


Fig. 8. Comparison of the group velocity between the FGPM layered structure ($p = -1$, $h_0/H = 0.2$) and the bilayer structure.

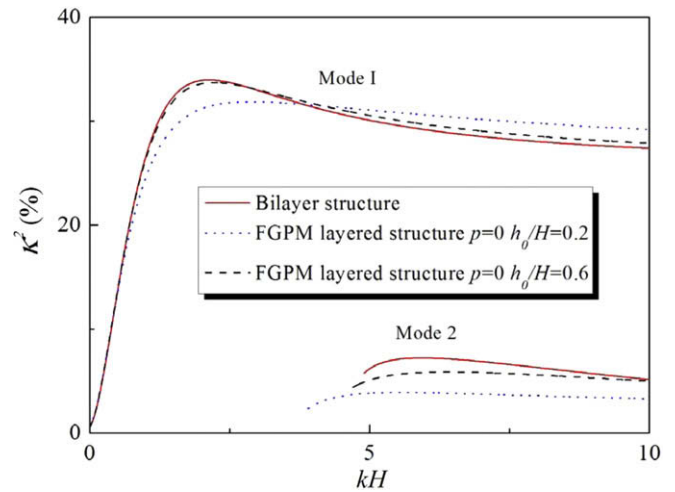


Fig. 9. Comparison of the electro-mechanical coupling factor.

4.3. Influence of gradient coefficient and top layer thickness on stress distributions

Fig. 12 shows the distribution of shear stresses along the thickness direction for the electrically open case, with the amplitude of the displacement on the surface fixed at $1 \mu\text{m}$, the gradient coefficient p equal to zero, $kH = 2\pi$ and $h_0/H = 0.6$ (i.e., the traction free surface is at $x/H = -0.6$). The results for a bilayer structure are also included in Fig. 12, for comparison. Note that there exists two interfaces in the FGPM composite structure located at $x/H = 0$ and $x/H = 0.8$, respectively, whereas only one interface exists in the two-layered structure at $x/H = 0.4$. By comparing the shear stress distributions at $kH = 2\pi$, it is seen that for the ungraded bilayer structure, the shear stress τ_{xz} changes abruptly and discontinuously at the interface ($x/H = 0.4$) for both mode 1 (Fig. 12a) and mode 2 (Fig. 12c). It is obvious from Fig. 12 that this discontinuity of shear stress can be eliminated by using the FGPM buffer layer.

5. Conclusions

In this work, the problem of the propagation of Love waves on the free surface of a three-layer FGPM composite structure is solved analytically. The power series technique is employed for

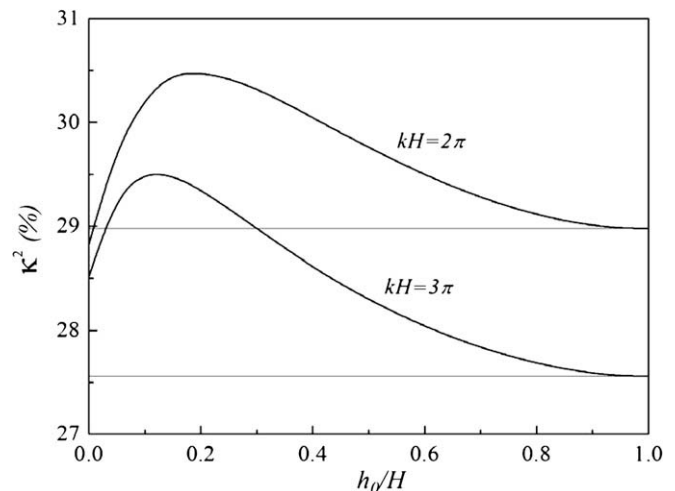


Fig. 10. Relations between the electro-mechanical coupling factor and h_0/H .

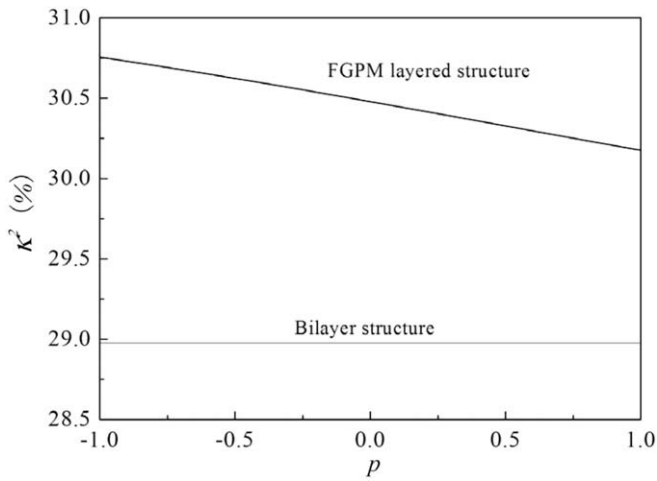


Fig. 11. Relations between the electro-mechanical coupling factor and p .

solving the differential equations with variable material coefficients. The influence of the material gradients on the dispersion relations of Love waves is systematically investigated.

Numerical examples indicate that the propagation properties in the FGPM composite structure are not only determined by the gra-

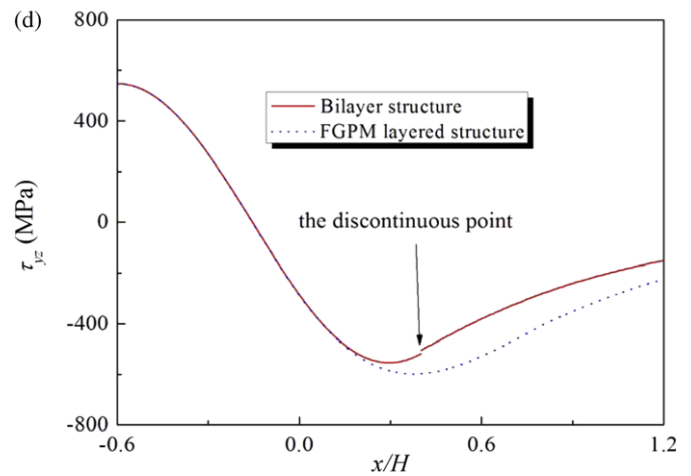
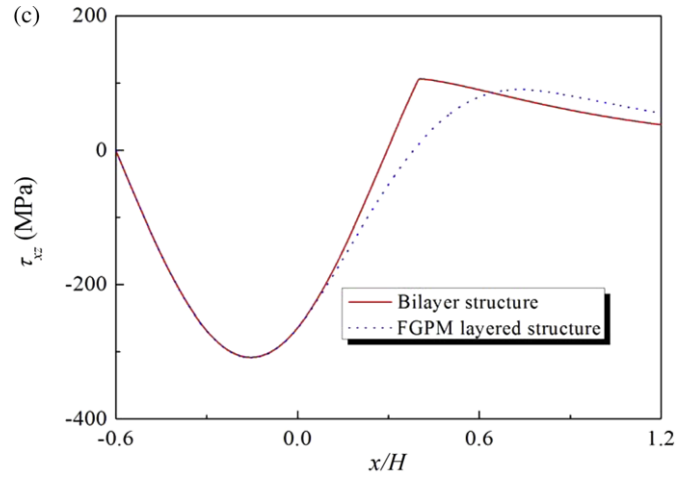


Fig 12. (continued)

dent coefficient and the thickness of the FGPM layer, but also by the electrical boundary conditions and the equivalent thickness. It is demonstrated that the adoption of a FGPM middle layer is very useful for improving the efficiency and durability of SAW devices. On one hand, the FGPM layer acts as a buffer layer and can avoid the stress discontinuity of the interface; a lower gradient coefficient and a suitable ratio of the top layer thickness to the FGPM layer thickness can improve the electro-mechanical coupling factor of the system. On the other hand, by combining the relation between wave number and gradient coefficient with the variations in Love wave velocities, a theoretical foundation can be provided for characterizing the material gradient coefficient through experimental measurements.

Acknowledgements

The authors gratefully acknowledge financial support from the National Basic Research Program of China (No. 2006CB601202), the National Natural Science Foundation of China (Nos. 10632060, 10825210), the National 111 Project of China (No. B06024), the Specialized Research Fund for the Doctoral Program of Higher Education of China (No. 20070698064) and the Program for New Century Excellent Talents in University (No. NCET-08-0429).

References

Cao, X., Jin, F., Wang, Z., 2008a. On dispersion relations of Rayleigh waves in a functionally graded piezoelectric material (FGPM) half-space. *Acta Mechanica* 200, 247–261.

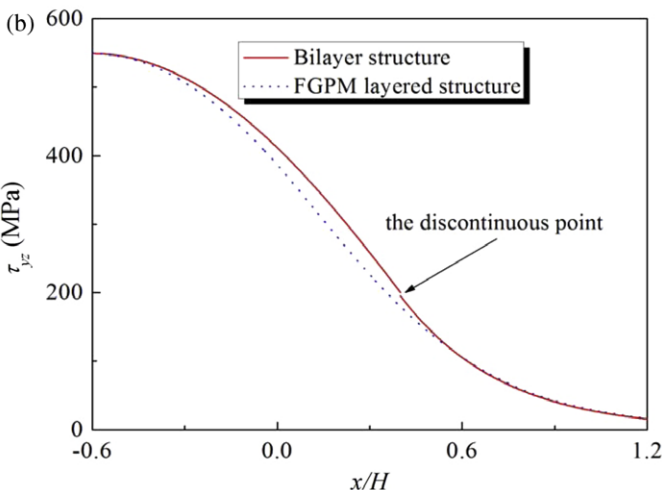
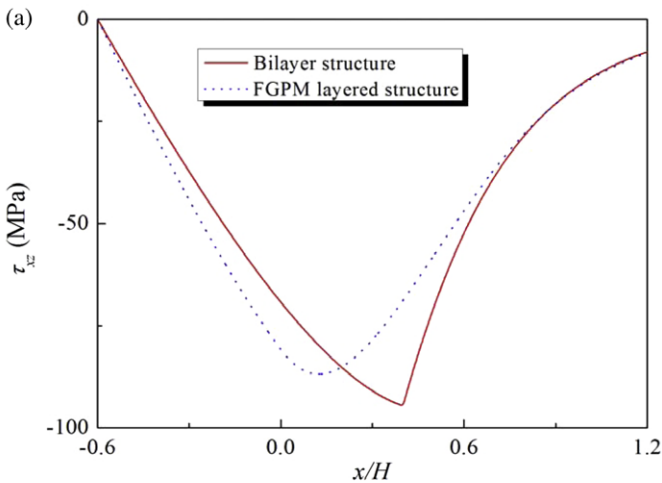


Fig. 12. The stress distributions of the first mode for the electrically open case at $kh = 2\pi$. (a) τ_{xz} of Mode 1, (b) τ_{yz} of Mode 1, (c) τ_{xz} of Mode 2 and (d) τ_{yz} of Mode 2.

- Cao, X., Jin, F., Wang, Z., 2008b. Theoretical investigation on horizontally shear waves in a functionally gradient piezoelectric material plate. *Advanced Materials Research*, 707–712.
- Collet, B., Destrade, M., Maugin, G.A., 2006. Bleustein–Gulyaev waves in some functionally graded materials. *European Journal of Mechanics – A/Solids* 25, 695–706.
- Du, J., Jin, X., Wang, J., Xian, K., 2007. Love wave propagation in functionally graded piezoelectric material layer. *Ultrasonics* 46, 13–22.
- Han, X., Liu, G.R., 2003. Elastic waves in a functionally graded piezoelectric cylinder. *Smart Materials and Structures* 12, 962–971.
- Han, X., Liu, G.R., Lam, K.Y., Ohyoshi, T., 2000. A quadratic layer element for analyzing stress waves in FGMs and its application in material characterization. *Journal of Sound and Vibration* 236, 307–321.
- Han, X., Liu, G.R., Lam, K.Y., 2001. Transient waves in plates of functionally graded materials. *International Journal for Numerical Methods in Engineering* 52, 851–865.
- Han, X., Liu, G.R., Xi, Z.C., Lam, K.Y., 2002. Characteristics of waves in a functionally graded cylinder. *International Journal for Numerical Methods in Engineering* 53, 653–676.
- Jin, F., Qian, Z.H., Wang, Z.K., Kishimoto, K., 2005. Propagation behavior of Love waves in a piezoelectric layered structure with inhomogeneous initial stress. *Smart Materials & Structures* 14, 515–523.
- Liu, G.R., Han, X., Lam, K.Y., 1999. Stress waves in functionally gradient materials and its use for material characterization. *Composites B* 30, 383–394.
- Liu, G.R., Tani, J., Ohyoshi, T., 1991. Lamb waves in a functionally gradient material plates and its transient response. Part 1: Theory; Part 2: Calculation result. *Transactions of the Japan Society of Mechanical Engineers* 57 (A), 131–142.
- Liu, H., Kuang, Z.B., Cai, Z.M., Wang, T.J., Wang, Z.K., 2003. Propagation of surface acoustic waves in prestressed anisotropic layered piezoelectric structures. *Acta Mechanica Sinica* 16, 16–23.
- Liu, J., Cao, X.S., Wang, Z.K., 2007. Propagation of Love waves in a smart functionally graded piezoelectric composite structure. *Smart Materials and Structures* 16, 13–24.
- Li, X.Y., Wang, Z.K., Huang, S.H., 2004. Love waves in functionally graded piezoelectric materials. *International Journal of Solids and Structures* 41, 7309–7328.
- Qian, Z., Jin, F., Wang, Z., Kishimoto, K., 2007. Transverse surface waves on a piezoelectric material carrying a functionally graded layer of finite thickness. *International Journal of Engineering Science* 45, 455–466.
- Wang, Q., Varadan, V.K., 2002. Wave propagation in piezoelectric coupled plates by use of interdigital transducer. Part 2: Wave excitation by interdigital transducer. *International Journal of Solids and Structures* 39, 1131–1144.
- White, R.M., Voltmer, F.W., 1965. Direct piezoelectric coupling to surface elastic waves. *Applied Physics Letters* 7, 314–316.